Confined swirling jet impingement on a flat plate at moderate Reynolds numbers

M. A. Herrada,[1] C. Del Pino,[2] and J. Ortega-Casanova[2]
[1]*Escuela Superior de Ingenieros, Universidad de Sevilla, Camino de los Descubrimientos s/n, Seville 41092, Spain*
[2]*E. T. S. Ingenieros Industriales, Universidad de Málaga, Pza. El Ejido s/n, Málaga 29013, Spain*

(Received 7 July 2008; accepted 20 November 2008; published online xx xx xxxx)

The behavior of a swirling jet issuing from a pipe and impinging on a flat smooth wall is analyzed numerically by means of axisymmetric simulations. The axial velocity profile at the pipe outlet is assumed flat while the azimuthal velocity profile is a Burger's vortex characterized by two dimensional parameters; a swirl number S and a vortex core length δ. We concentrate on the effects of these two parameters on the mechanical characteristics of the flow at moderate Reynolds numbers. Our results for $S=0$ are in agreement with Phares *et al.* [J. Fluid Mech. **418**, 351 (2000)], who provide a theoretical determination of the wall shear stress under nonswirling impinging jets at high Reynolds numbers. In addition, we show that the swirl number has an important effect on the jet impact process. For a fixed nozzle-to-plate separation, we found that depending on the value of δ and the Reynolds number Re, there is a critical swirl number, $S=S^*(\delta,\mathrm{Re})$, above which recirculating vortex breakdown bubbles are observed in the near axis region. For $S>S^*$, the presence of these bubbles enhances the transition from a steady to a periodic regime. For $S<S^*$, the flow remains steady and the results show that the introduction of swirl reduces the maximum pressure and radial skin-friction coefficients over the wall.
[DOI: 10.1063/1.3063111]

I. INTRODUCTION

The impingement of a submerged jet on a smooth solid surface is a problem of great importance in many engineering applications (cooling, heating, and drying processes, sealing of materials, underwater cleaning, among others). The wall shear stress and heat transfer properties of submerged jets are crucial to determine their efficiency and, therefore, to predict their potential impact on the process.

Although turbulent jets are used in most of these applications, specially those related to the heat transfer phenomenon, valuable insight is obtained from the study of laminar impinging jets. In particular, some authors have focused on the mechanical behavior of laminar jets. Salient examples are the characterization of the skin-friction coefficient,[1,2] the boundary layer separation at the wall,[3,4] and the influence of the velocity profiles on the flow pattern close to the impingement area.[5,6] Particularly interesting is the work of Phares *et al.*,[1] providing a method for the theoretical determination of the wall shear stress under diverse impinging jet setups. Moreover, submerged jets emerging from a nozzle with an axial uniform flow and impinging onto a flat plate have been experimentally and numerically studied,[4] and the nozzle-to-plate separation (jet height) is rescaled to yield a collapse of the data onto a single curve independent of the Reynolds number. The attractiveness of impinging jets has increased recently owing to such industrial applications, at moderate Reynolds numbers, as portable computer cooling[7] and atherogenesis research by means of endothelial surface tests.[8–10]

Despite the significant number of works dealing with jet impingement on a plane, less attention is paid to the swirl effect at moderate Reynolds number. Most research on impinging swirling jets focuses on the heat transfer characteristics of the flow. For example, some experimental works with turbulent swirling flows[11–13] show that swirling jets improve heat transfer significantly in comparison to turbulent jets without swirl.[14,15] At high Reynolds numbers, helical waves are always dominant in the shear layer of swirling jet flows, either with or without vortex breakdown (VB); this is well documented in a series of experimental and computational works.[16–20] Helicoidal waves were also observed in an experimental setup with impinging turbulent swirling jet flows.[21] However, at moderate Reynolds number, the importance of helicoidal waves in the general structure of the flow is much smaller, and in many instances the flow can be described as strictly axisymmetric. An example is the work of Sanmiguel-Rojas *et al.*[22] where it was shown that the three-dimensional swirling flow discharging in a sudden expansion becomes basically axisymmetric when the swirl parameter attains a threshold where VB takes place. Herrada and Fernández-Feria[23] studied the development of VB in a straight pipe flow without wall friction. The transition to helical breakdown modes was shown to issue from an upstream axisymmetric recirculation region (bubble or vortex core). Therefore, a purely axisymmetric stability analysis can yield significant insight into the vortex dynamics of jet and columnar flows.

Axisymmetric simulations have been used in the past to describe the thermal aspects of impinging swirling jet flows at moderate Reynolds numbers.[24,25] Our main objective in this work is to study the interaction between impinging (non-

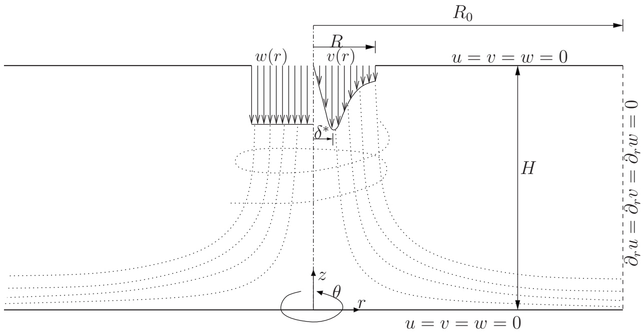

FIG. 1. Basic flow geometry.

swirling and swirling) jets and a solid wall in a confined domain at moderate Reynolds numbers; our attention will focus on the dynamics of the flow, aiming at the description of the swirl influence on the mechanics of impingement (pressure, shear) and on the flow pattern (specifically, bubble structure). These are the dominant mechanical characteristics of the impinging jet and, therefore, have an important influence on the effectiveness of its potential applications (computer cooling, atherogenesis treatment).

In particular, for a fixed geometrical configuration, we identify the parametric region where recirculating bubbles (with reverse axial flow) are to be expected in the flow. We show that the occurrence of recirculating bubbles, hereafter referred to as VB bubbles, is a key factor determining the mechanical characteristics of the impinging jet. To that end, axisymmetric calculations will be carried out to determine the skin-friction and pressure coefficients at the wall. Furthermore, we will analyze the mechanics of the flow as a function of three main parameters: the Reynolds number, the swirl parameter, and the vortex core radius.

This paper is organized as follows. First, a general problem formulation and a description of the numerical scheme are included in Sec. II. The presentation of axisymmetric numerical results, the comparison with a previous nonswirling jet study, are given in Sec. III. A summary of the main results is presented in Sec. IV.

II. FORMULATION OF THE PROBLEM

Incompressible, axisymmetric and time-dependent dimensional Navier–Stokes equations describing the dynamics of a (swirling or nonswirling) impinging jet are solved in cylindrical coordinates (r,θ,z). The jet emerges from a pipe of radius R and it impinges on a smooth wall located at a given distance H. The flow configuration and the computational domain are depicted in Fig. 1. To render the governing equations dimensionless, the pipe radius R and the maximum jet exit axial velocity W are used. The convective time scale is $T=R/W$, and the characteristic pressure is $P=\rho W^2$, where ρ is the constant density of the fluid. Using these characteristic parameters, the dimensionless continuity and momentum equations are written as

$$\frac{1}{r}\frac{\partial(ru)}{\partial r} + \frac{\partial w}{\partial z} = 0, \tag{1}$$

$$\frac{Du}{Dt} = -\frac{\partial p}{\partial r} + \frac{v^2}{r} + \frac{1}{\mathrm{Re}}\left[\nabla^2 u - \frac{u}{r^2}\right], \tag{2}$$

$$\frac{Dv}{Dt} = \frac{uv}{r} + \frac{1}{\mathrm{Re}}\left[\nabla^2 v - \frac{v}{r^2}\right], \tag{3}$$

$$\frac{Dw}{Dt} = -\frac{\partial p}{\partial z} + \frac{1}{\mathrm{Re}}[\nabla^2 w], \tag{4}$$

where (u,v,w) and p are the dimensionless velocity and pressure fields. The mathematical operators D/Dt and ∇^2 are defined as

$$\frac{D}{Dt} = \frac{\partial}{\partial t} + u\frac{\partial}{\partial r} + w\frac{\partial}{\partial z} \tag{5}$$

and

$$\nabla^2 = \frac{1}{r}\frac{\partial}{\partial r}\left(r\frac{\partial}{\partial r}\right) + \frac{\partial^2}{\partial z^2}. \tag{6}$$

The Reynolds number is defined in terms of ν, the kinematic viscosity of the fluid,

$$\mathrm{Re} = \frac{WR}{\nu}. \tag{7}$$

The above set of equations has been solved to describe the behavior of a family of swirling impinging jets issuing from a pipe outlet located at $z=H/R$. The dimensionless velocity field (u,v,w) at the pipe outlet is assumed to be

$$u = 0, \quad v = \frac{S}{r/\delta}\{1 - \exp[(-(r/\delta)^2)]\},$$
$$w = -1 \quad (0 \le r \le 1), \tag{8}$$

where $\delta=\delta^*/R$ is the characteristic dimensionless vortex core radius and S is a swirl parameter defined as

$$S = \frac{\Gamma}{W\delta^*}, \tag{9}$$

while Γ is the vortex circulation far from the axis $(r \gg \delta)$. The velocity profiles described in Eq. (8) combine a uniform axial flow and a circumferential (Burger's vortex) flow, with no radial flow. This velocity field is in good agreement with the inlet velocity of some experiments on VB in pipes,[26] and it has been extensively used in different theoretical and numerical investigations of axisymmetric swirling flows in pipes.[27,28] Here, the velocity field (8) imposed at the outlet pipe is used to study the effect of the swirl (S) and the size of the core (δ) on the behavior of the impinging jet.

At the solid boundaries ($z=0$ and $z=H/R$ with $r>1$), nonslip boundary conditions are imposed,

$$w = v = u = 0. \tag{10}$$

Finally, away from the jet impact region, at $r=R_o/R \gg 1$, outflow conditions are considered,

$$\frac{\partial w}{\partial r} = \frac{\partial v}{\partial r} = \frac{\partial u}{\partial r} = 0. \tag{11}$$

Most of the axisymmetric numerical results reported are obtained for a single jet height $H/R=10$. This is a typical distance used in seabed excavations applications based on impinging swirling jets.[29] However, in order to compare with previous results for nonswirling jets,[1] some simulations have been performed with a different jet height ($H/R=16$, see Sec. III). In addition to this, a sufficiently large outer radius R_o has been selected to ensure that the outflow boundary conditions (11) do not affect the results. Thus, $R_o/R=60$ in all the simulations presented here.

A. Computational method

To compute the time evolution, a mixed implicit-explicit second order projection scheme based on backward differentiation is used.[30] The spatial discretization in the (z,r) coordinates (meridional plane) is carried out with n_r and n_z Chebyshev spectral collocation points in the radial and axial coordinates (r,z). This approximation allows us to use the matrix diagonalization method,[31] whose computational complexity is of the order of $n_r \times n_z \times \min(n_r,n_z)$. The resulting set of three Helmholtz-type (momentum) equations is solved, along with the Poisson equation providing the pressure corrections. The geometry is chosen to be $R_o/R=60$ and $H/R=10$ (in addition, $H/R=16$ is explored in the case $S=0$). We have carried out the numerical simulations in a grid with $n_r=200$, $n_z=61$ for the range of swirl parameters and the moderate Reynolds numbers (7) considered in this work. Several convergence tests have been run in finer grids (with $n_r=301$, $n_z=81$), suggesting that this resolution level provides accurate results. The time step employed in most of the simulations was $\Delta t=0.01$. No significant differences in the temporal evolution of the flow were found using smaller time steps, in particular, for those cases where a pure periodic unsteady regime was found (see Sec. III).

III. RESULTS

In order to quantify the mechanical effects of the impinging jet on the wall, let us introduce the radial and azimuthal skin-friction coefficients defined as

$$c_{\mathrm{fr}}(r) = \frac{\tau^*_{z^*r^*}(z=0,r)}{\rho W^2} = \frac{1}{\mathrm{Re}}\left(\frac{\partial u}{\partial z} + \frac{\partial w}{\partial r}\right)_{z=0,r} = \frac{1}{\mathrm{Re}}\frac{\partial u}{\partial z}, \quad (12)$$

$$c_{f\theta}(r) = \frac{\tau^*_{z^*\theta}(z=0,r)}{\rho W^2} = \frac{1}{\mathrm{Re}}\left(\frac{\partial v}{\partial z} + \frac{1}{r}\frac{\partial w}{\partial \theta}\right)_{z=0,r} = \frac{1}{\mathrm{Re}}\frac{\partial v}{\partial z}, \quad (13)$$

where $\tau^*_{z^*r^*}$ and $\tau^*_{z^*\theta}$ are the two-dimensional components of the stress tensor tangent to the wall surface $z=0$.

The pressure coefficient over the wall is also defined as

$$c_p(r) = \frac{p^*(z=0,r) - p^*(z=0,r\to\infty)}{\rho W^2}$$

$$= p(z=0,r) - p(z=0,R_o/R), \quad (14)$$

where "$*$" denotes dimensional variables. The discussion that follows analyzes the above quantities and the general structure of the flow for nonswirling ($S=0$) and swirling ($S>0$) cases, respectively, for a range of Reynolds numbers, $50\leq \mathrm{Re}\leq 500$.

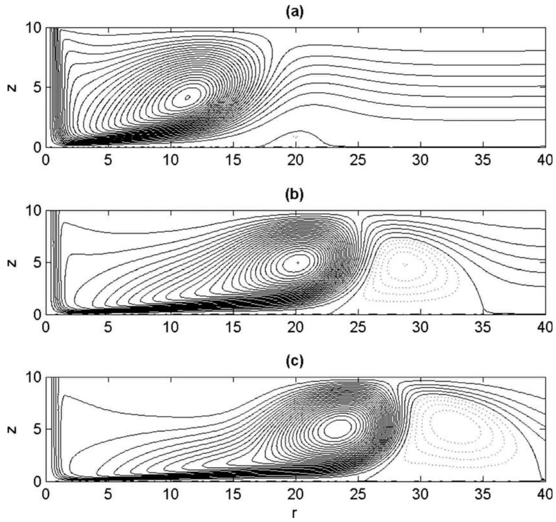

FIG. 2. Streamlines of a nonswirling jet ($S=0$) for different Reynolds numbers: Re=100 (a), Re=300 (b), and Re=500 (c). Dotted lines represent the separation region.

A. Nonswirling jet ($S=0$)

First, the nonswirling jet impingement on a flat wall is considered. The axisymmetric numerical simulations presented here show that, starting from rest, the flow reaches a steady state. The streamlines for three Reynolds numbers and $H/R=10$ are shown in Fig. 2 [Re=100 (a), Re=300 (b), and Re=500 (c)]. It can be observed that there is a large recirculating area associated with the impinging process; the size of this cell increases as the Reynolds number increases. Added to this, the separation between streamlines near the wall decreases as the Reynolds number increases, indicating a strong velocity gradient near the wall where a boundary layer develops. This boundary layer that moves the wall apart develops along the radial coordinate and separates from the wall at a given radial position r_{sep}. At a further radial position, the flow is reattached to the wall. Dotted lines in Fig. 2 show streamlines within the separation region. Clearly, this region becomes wider when the Reynolds number increases. To determine the separation point r_{sep} the condition $c_{fr}(r_{\mathrm{sep}})=0$ is used. Figure 3 shows r_{sep} as function of the Reynolds number. In the range of Reynolds numbers analyzed, r_{sep} grows as the Reynolds number increases. It is known that r_{sep} grows asymptotically to a constant value as the Reynolds number is increased, since the position where the boundary layer separation takes places should become independent of the Reynolds numbers when the near-wall boundary layer is fully developed. On the other hand, no separation was found below $\mathrm{Re}\approx 85$.

Let us now focus our attention on the dynamics of the jet in the impingement region. Figures 4(a) and 4(b) represent c_{fr} and c_p as a function of r for the three cases considered in Fig. 2. Figure 4(a) shows that c_{fr} increases from zero (at the axis, $r=0$) to a maximum value $c_{fr}^{\max}$, and then its value decays as r increases. An opposite trend is shown in Fig. 4(b),

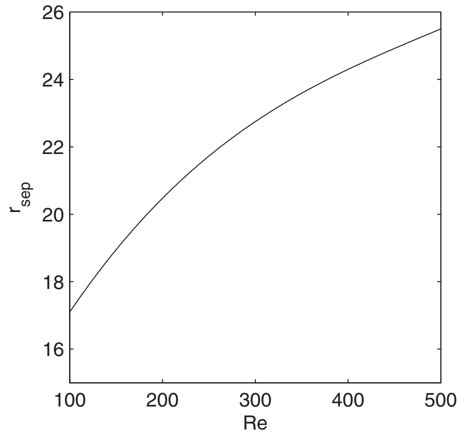

FIG. 3. r_{sep} as a function of Re.

where c_p decays monotonically with r and achieves a maximum value c_p^{max} at $r=0$. As expected, c_p^{max} tends to a constant value, while c_{fr}^{max} decays, when Re increases. On the other hand, the skin-friction coefficient can be rescaled to be independent of the Reynolds number. In fact, Phares *et al.*[1] predicted that, for high Reynolds numbers, $\mathrm{Re} \gg 1$, the wall shear stress $[\tau = (\tau^*_{z^* r^*})_{z=0}]$ in a laminar boundary layer (axisymmetric case) can be scaled according to the law

$$\frac{\tau\sqrt{2\,\mathrm{Re}}(H/2R)^2}{\rho W^2} = f(Rr/H, H/R), \tag{15}$$

where function f is an analytical expression which only depends on the variable Rr/H and the jet height H/R. To validate our results, we have plotted in Fig. 5 the rescaled function $\tau_P = \tau\sqrt{2\,\mathrm{Re}}(H/2R)^2/(\rho W^2)$ as a function of Rr/H for three different Reynolds numbers and two different jet heights. For $H/R=10$, Fig. 5(a) shows that the radial dependency of τ_P tends asymptotically to a unified curve as Re increases and its maximum value is reached at $rR/H \approx 0.16$. This radial coordinate is consistent with the theoretical prediction reported: 0.10 ($H/R=8$) and 0.2 ($H/R=12$), although no data are available for the case $H/R=10$.[1] Nevertheless, to guarantee the axisymmetric numerical results presented in this work, τ_P is represented again as a function of rR/H in Fig. 5(b) for a different jet height, $H/R=16$. This H/R value is located close to the asymptotic threshold where the wall shear stress starts to be self-similar.[1] For this jet height, good agreement between the numerical axisymmetric results and the theoretical predictions is found: τ_P tends asymptotically to the analytical curve[1] as the Reynolds number Re is increased; and the maximum wall shear stress is reached at $rR/H=0.09$, confirming the results previously known.

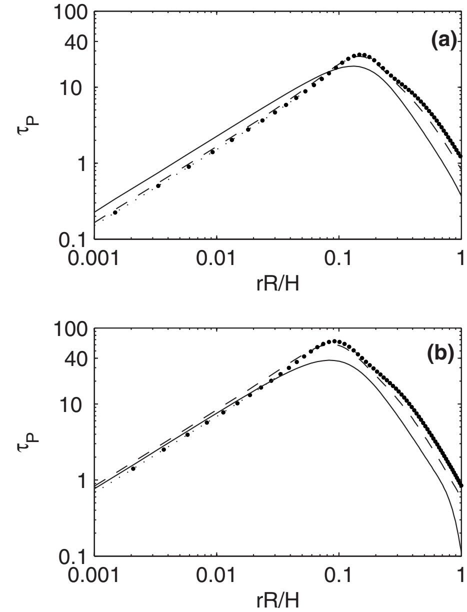

FIG. 5. τ_P as function of rR/H for $S=0$ and two values of the dimensionless distance to the wall H/R: $H/R=10$ (a) and $H/R=16$ (b). Three values of the Reynolds number are depicted in both cases Re=100 (solid lines), Re=300 (dashed lines), and Re=500 (dotted lines).

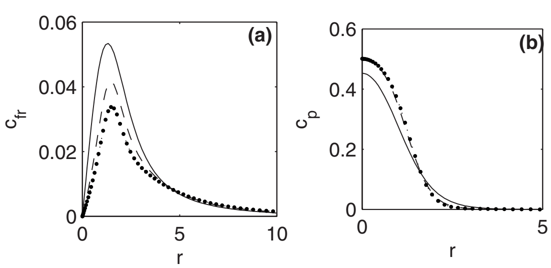

FIG. 4. (a) c_{fr} and (b) c_p as a function of r for $S=0$ and three values of Re: Re=100 (solid lines), Re=300 (dashed lines), and Re=500 (dotted lines).

B. Swirling jet ($S>0$)

The effect of swirl on the behavior of the impinging jet has been analyzed for a fixed jet height, $H/R=10$. In Sec. III A the results for a fixed value of the vortex core radius δ are described in detail. In Sec. III B, we will explore the effect of changing δ to illustrate the importance of this parameter on the structure and stability of the flow.

1. Results for $\delta=0.5$

Let us start by analyzing the structure of the flow for a fixed value of the vortex core radius, $\delta=0.5$. For $S=0.3$ the numerical axisymmetric results show that the axial flow does not differ much from the nonswirling flow. Figure 6 shows streamlines for the steady state solution for Re=100 (a), Re=300 (b), and Re=500 (c). It can be seen that the streamlines are similar to the streamlines in Fig. 2 for the case without swirl ($S=0$). Of course, $S \neq 0$ implies that there is an azimuthal motion superimposed on the axial flow. The circulation contours, $\Gamma = vr$, for these cases are shown in Figs. 6(d)–6(f). Note that the circulation is first convected by the jet from the pipe toward the wall, and then it is spread radially away from the axis owing to the strong radial flow created by the boundary layer in vicinity of the wall. Clearly, the convection of circulation becomes more effective as the Reynolds number increases, since it leads to a decrease in the relative importance of the viscous dissipation term.

The main effect of increasing the circulation advection, for a fixed value of the Reynolds number, is to produce a significant drop of the maximum values of the pressure and

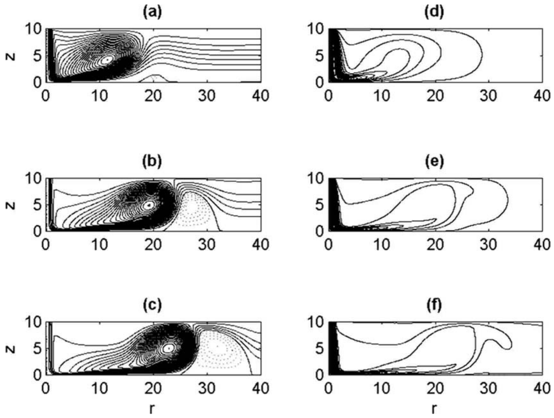

FIG. 6. Streamlines for a swirling jet with $S=0.3$, $\delta=0.5$, and Re=100 (a), Re=300 (b), and Re=500 (c). Dotted lines represent the separation region. Circulation isocontours Γ [Re=100 (d), Re=300 (e), and Re=500 (f)].

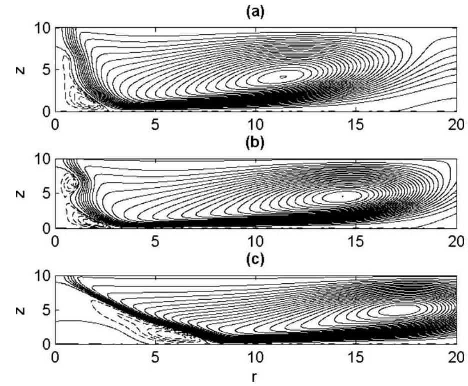

FIG. 8. Streamlines for a swirling jet with $S=0.6$, $\delta=0.5$, and Re=100 (a), Re=150 (b), and Re=200 (c). Dotted lines represent the VB bubble.

radial skin-friction coefficients at the wall. This is shown in Fig. 7, where we plot the skin-friction and pressure coefficients for the steady state solution under three different swirl parameters ($S=0.2$, 0.3, and 0.4) and a fixed value of the Reynolds number, Re=300. Note that $c_{fr}^{\max}$ and $c_p^{\max}$ decrease as S grows. Added to this, the maximum value of the azimuthal skin-friction coefficient at the wall ($c_{f\theta}^{\max}$) increases with S. It is worth noting that the locus of $c_p^{\max}$ moves from the axis to a radial position $r>0$, which is $r\approx 1.3$ for $S=0.4$. The figure also shows that for $S=0.4$ there is a small region near the axis where the radial skin-friction coefficient becomes negative. These two facts can be explained owing to the presence of a small recirculating bubble near the axis with reverse flow (positive velocity at the axis). These VB bubbles are similar to the bubbles observed experimentally and computed numerically in a completely filled, enclosed, circular cylinder driven by a constant angular velocity in the end wall.[32,33] Our case shares with the above references the basic flow pattern, a swirling jet impinging on a wall. Nevertheless, the confined cylinder problem[32,33] is characterized by a nonrotating wall: as a result, the axial and azimuthal motions are not independent.

Other similarities with the flow in an enclosed cylinder are analyzed. The VB bubbles can spread over all the near-axis region when the swirl intensity is sufficiently high. For instance, Fig. 8 depicts instantaneous streamlines for $S=0.6$ and Re=100 (a), Re=150 (b), and Re=200 (c). While in the two first cases [(a) and (b)] the flow has reached a steady solution, in the last one (c) the flow has evolved into a purely periodic unsteady regime. Note that the VB bubble (dashed lines) changes its shape when the Reynolds number increases, reaching a nearly conical shape for Re=200. The maximum axial velocity of the solution in the domain is defined as

$$w_{\max} = \max[w(r,z)]_{0\le r\le R_o, 0\le z\le H}, \tag{16}$$

the time periodic character of the flow for Re=200 can be seen in Fig. 9, where $w_{\max}$ is plotted as a function of time. Note that for the remaining intensive swirl instances considered, w reaches its maximum value at some point within the VB bubbles. The initial condition used in the simulation is the steady solution obtained for Re=150; the oscillation frequency ω is about 0.2.

2. The effect of changing δ on the structure of the flow

The above results clearly show that the presence of reverse flow in the axial region has an important effect on both the structure and the stability of the flow. In particular, we find that the presence of the VB bubbles leads to negative radial skin friction at the wall, close to the axis. In addition, the maximum pressure coefficient $c_p^{\max}$ is not located at the axis, $r=0$. Therefore, it is interesting to determine the threshold curve for which no VB bubbles are present. To that end, for a given Re we have found the maximum value of the swirl parameter, critical value S^*, for which no reverse flow occurs at any point of the axis. The result of this process in the (Re,S)-plane is shown in Fig. 10, where the neutral curve

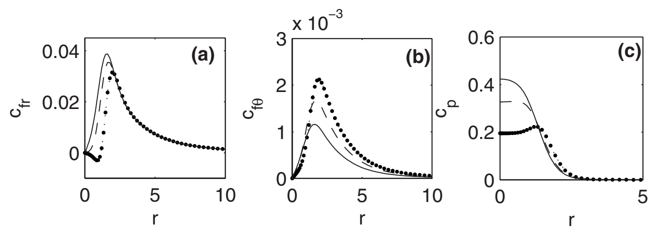

FIG. 7. c_{fr} (a), $c_{f\theta}$, (b) and c_p (c) as a function of r for Re=300, $\delta=0.5$ and three values of S: $S=0.2$ (solid lines), $S=0.3$ (dashed lines), and $S=0.4$ (dotted lines).

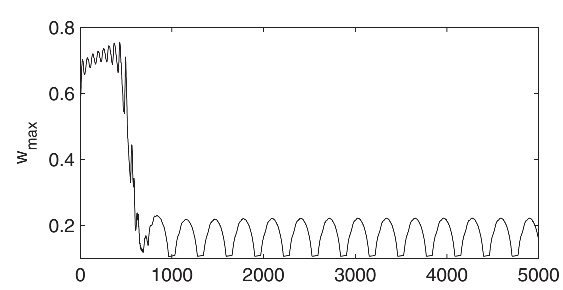

FIG. 9. Time evolution of the maximum value of the axial velocity for $S=0.6$, $\delta=0.5$, and Re=200.

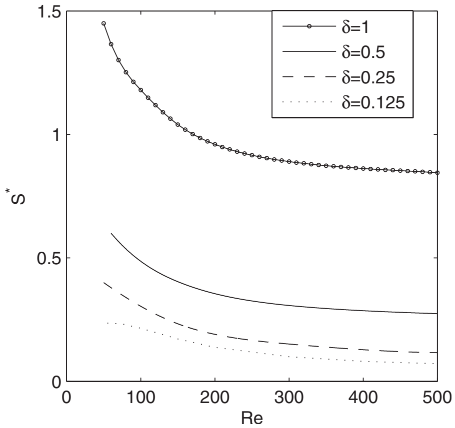

FIG. 10. Critical swirl parameter as function of Re for four different vortex core radii.

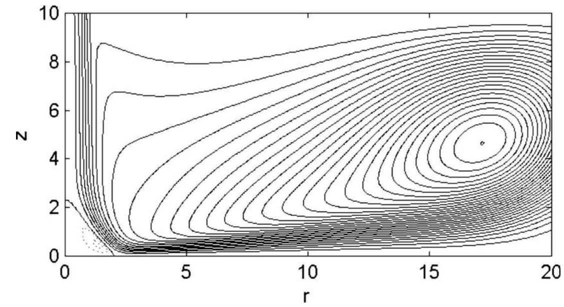

FIG. 11. Streamlines for a swirling jet with $S=0.3$, $\delta=0.25$, and Re=200.

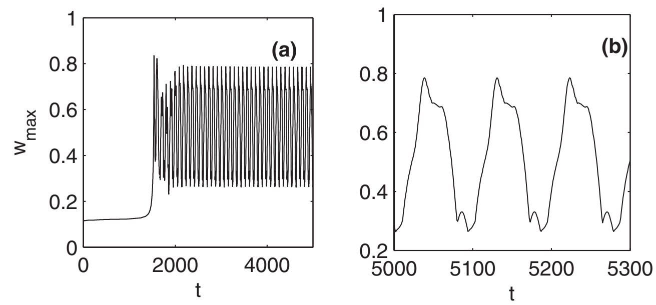

FIG. 12. (a) Time evolution of the maximum value of the axial velocity for $S=0.3$, $\delta=0.25$, and Re=204. (b) Detail of the evolution for $5000 \leq t \leq 5300$.

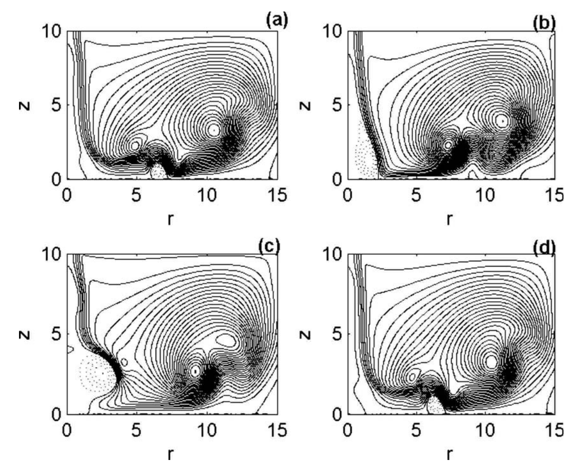

FIG. 13. Instantaneous streamlines for a time-dependent case with $S=0.3$, $\delta=0.25$, and Re=204 at different times (a) $t=5000$, (b) $t=5030$, (c) $t=5060$, and (d) $t=5090$.

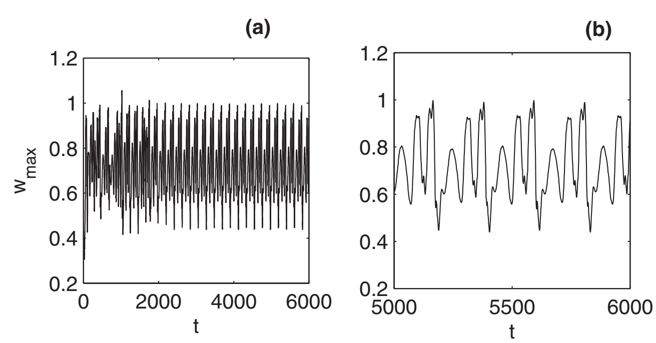

FIG. 14. (a) Time evolution of the maximum value of the axial velocity for $S=0.3$, $\delta=0.125$, and Re=200. (b) Detail of the evolution for $5000 \leq t \leq 6000$.

S^* as a function of Re is depicted for four different vortex core radii. When the vortex core radius is reduced, the swirl intensity required to achieve the axisymmetric VB bubble near the axis decreases, as shown in Fig. 10. Below the neutral curve, a steady flow with no VB bubbles is ensured for the Reynolds number range considered in this work. Above the neutral curve, VB bubbles exist and their time-dependent structures are strongly affected by the values of the swirl parameter and the Reynolds number. For instance, to illustrate the pattern diversity, we first show a steady VB bubble solution for Re=200, $\delta=0.25$, and $S=0.3$ (see Fig. 11). This steady solution becomes time periodic when the Reynolds number increases. Figure 12 shows the time evolution of $w_{\max}$ when the Reynolds number is suddenly increased from an initially steady flow with Re=202 to Re=204. Figure 12 shows that the oscillation frequency is 0.069 and that $w_{\max}$ does not follow a pure oscillation (it has two local minimum and maximum values in each oscillation period). This time-dependent behavior is explained because in addition to the near-axis VB bubble, an additional, small recirculating bubble appears close to the wall but away from the axis. Both bubbles show up and disappear sequentially, and the interaction between their pulses produces the final modulated wave (see Fig. 12).

Figure 13 shows instantaneous streamlines for the case Re=204, $\delta=0.25$, and $S=0.3$ at four different times: (a) $t=5000$, (b) $t=5030$, (c) $t=5060$, and (d) $t=5090$, to illustrate this example. To our knowledge, no experimental data are available showing this axisymmetric oscillating (double bubble) flow structure. We have found double bubbles only in impinging jets with sufficiently small values of δ. For example, Fig. 14 shows the time behavior of $w_{\max}$ for a flow with Re=200, $\delta=0.125$, and $S=0.3$. In this case again, an imperfectly periodic regime is reached once the swirl parameter is changed from $S=0.25$ (where a steady flow exists) to $S=0.3$. Instantaneous streamlines for this case (see Fig. 15) show again the presence of near-wall bubbles. This bubble pattern is peculiar and has not been described elsewhere, to our knowledge. They are intermittent (they show up and vanish periodically), while a permanent near-axis (VB) bubble is observed in the simulation domain. However, near-wall

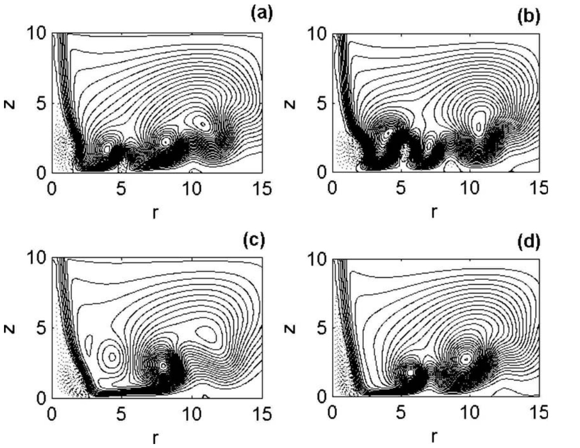

FIG. 15. Instantaneous streamlines for a time-dependent case with $S=0.3$, $\delta=0.125$, and $\text{Re}=200$ at different times (a) $t=5400$, (b) $t=5455$, (c) $t=5510$, and (d) $t=5565$.

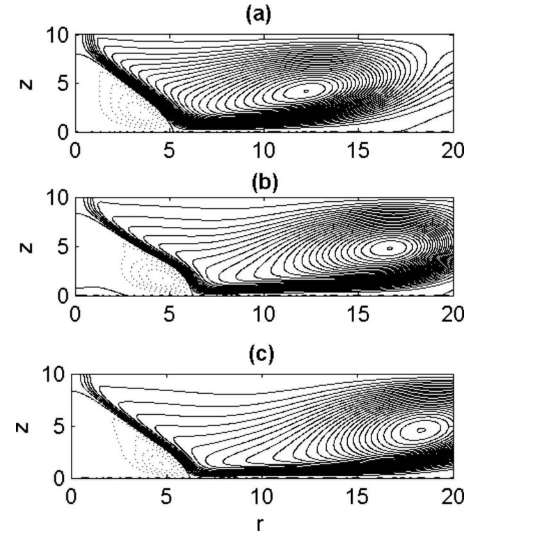

FIG. 16. Instantaneous streamlines for a swirling jet with $S=1.4$, $\delta=1$, and $\text{Re}=100$ (a), $\text{Re}=200$ (b), and $\text{Re}=250$ (c).

bubbles are not present when the vortex core radius is large enough. For example, Fig. 16 depicts instantaneous streamlines for $S=1.4$, $\delta=1$, and $\text{Re}=100$ (a), $\text{Re}=200$ (b), and $\text{Re}=250$ (c). While in the first two cases [(a) and (b)] the flow has reached a steady solution, in the last one (c) the flow has developed a pure periodic unsteady regime (see Fig. 17). Observe that, like for the case $\delta=0.5$, for $\delta=1$ a big VB bubble exists if the swirl parameter is large enough. Another similarity is that the steady flow with the VB bubble becomes time periodic (with a pure period) when the Reynolds number is increased. As previously shown, the situation is different for smaller values of δ ($\delta=0.5$ and $\delta=0.25$), where the growth of either the swirl parameter or the Reynolds number can yield an unsteady imperfect periodic flow if the steady flow has initially a VB bubble.

On the other hand, the effect of S and δ on the impinging properties of the flow is studied. Keeping Re and δ constant, we find that the maximum values of the radial skin-friction and pressure coefficients decrease as the swirl parameter S increases. This can be seen in Fig. 18 where the skin-friction and pressure coefficients are plotted for the steady state solution, assuming $\text{Re}=200$, $\delta=0.25$, and three different swirl parameters. Furthermore, the figure shows that the maximum value of the azimuthal skin factor increases as S increases. Keeping Re and S fixed, it is also possible to reduce the maximum value of the radial skin-factor and pressure coefficients by decreasing δ. In effect, Fig. 19 shows the skin-friction and pressure coefficients as a function of r for the steady state solution corresponding to $\text{Re}=200$, $S=0.3$, and three different vortex core radii. Note than in this case, the maximum value of the azimuthal skin-factor coefficient increases as δ decreases.

Finally, we apply the scaling law (15) to cases where VB bubbles are not present. For a given δ, we shall select a swirl parameter S such that $S<S^*(\text{Re}\to\infty,\delta)$. The choice is made in order to have limited swirl so that the flow remains steady when sufficiently high Reynolds numbers are selected. This analysis allows us to study the effect of swirl on the rescaled radial shear stress τ_P. Figure 20(a) shows τ_P as a function of rR/H for $\delta=1$ and $S=0.3$ and three different Reynolds num-

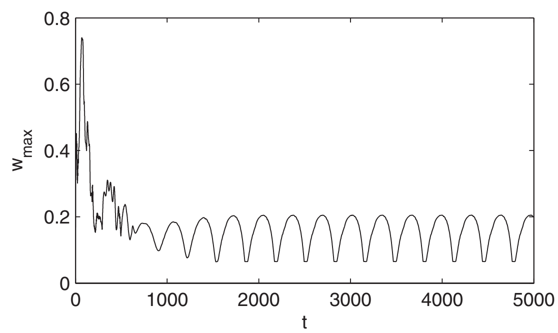

FIG. 17. Time evolution of the maximum value of the axial velocity for $S=1.4$, $\delta=1$, and $\text{Re}=250$.

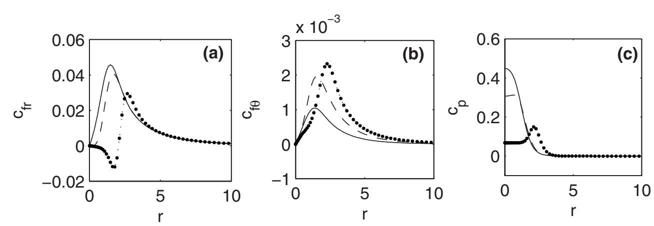

FIG. 18. (a) c_{fr}, (b) $c_{f\theta}$, and (c) c_p as a function of r for $\text{Re}=200$, $\delta=0.25$, and three values of S: solid lines $S=0.1$, dashed lines $S=0.2$, and dotted lines $S=0.3$.

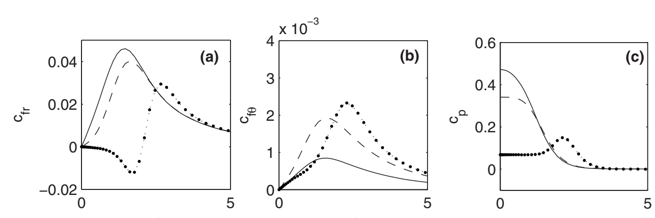

FIG. 19. (a) c_{fr}, (b) $c_{f\theta}$, and (c) c_p as a function of r for $\text{Re}=200$, $S=0.3$, and three values of δ: solid lines $\delta=1$, dashed lines $\delta=0.5$, and dotted lines $\delta=0.125$.

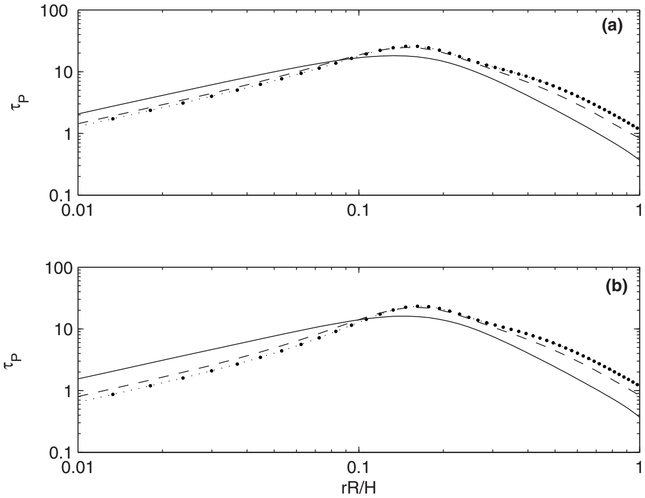

FIG. 20. τ_P as a function of rR/H for $\delta=1$ and two values of S:$S=0.3$ (a) and $S=0.6$ (b). Three values of the Reynolds number are depicted in both cases Re=100 (solid lines), Re=300 (dashed lines), and Re=500 (dotted lines).

bers, while Fig. 20(b) corresponds to a different swirl parameter, $S=0.6$. As expected, in both cases, τ_P tends asymptotically to an unique curve as Re increases. Interesting enough is the fact that in both asymptotic curves, the maximum value of the radial shear stress $\tau_P^{\max}$ is reached at the same radial position, $r/H \sim 0.16$, as in the nonswirling case. The main difference between the asymptotical curves ($S=0$, $S=0.3$, and $S=0.6$) is the following: in the region $rR/H < 0.16$, τ_P and $\tau_P^{\max}$ decrease as S increases. The same behavior is observed when a different value of δ is selected; $\tau_P^{\max}$ is reached at $rR/H \sim 0.16$ for high Reynolds numbers and its value decreases with S.

Although no experimental data are available for the swirling jet impingement at moderate Reynolds numbers, our results qualitatively agree with the numerical data obtained by Owsenek *et al.*[24] for a different flow configuration. In that work, it was shown that axial jets similar to the jets considered in our work have a pressure coefficient and a local Nusselt number (directly related to the skin-factor coefficient) at the wall which decrease as the swirl increases.

IV. SUMMARY AND CONCLUSIONS

The axisymmetric flow structure of swirling impinging jets that emerge from a pipe that is aligned at a fixed distance normal to the wall has been analyzed numerically. The fundamental mechanisms to know the influence of the jet impingement onto the wall are quantified by means of the skin-friction and pressure coefficients defined along the wall.

The results for nonswirling flows ($S=0$) are in agreement with a theoretical model providing a scaling law for the shear wall stress at the wall at high Reynolds numbers, $\mathrm{Re} \gg 1$.

The effect of swirl intensity (S) and vortex core radius (δ) on the behavior of the impinging jet has been analyzed for a constant jet height, $H/R=10$. The results show that the presence of reverse flow in the axis region associated with the swirl has an important effect on both the structure and the stability of the flow. The maximum swirl intensity compatible with no reverse flow anywhere at the axis, $S^*(\delta,\mathrm{Re})$, has been computed for several values of δ in the range of Reynolds numbers considered in this work, showing that the larger the value of δ, the larger the swirl intensity required to get VB bubbles in the near-axis region.

For $S<S^*$ the flow remains steady and the effect of swirl on the scaling law modeling the radial shear stress has been studied. The results show that the rescaled wall shear stress reaches its maximum value, $\tau_P^{\max}$, at the same location for both swirling and nonswirling jets. Additionally, $\tau_P^{\max}$ decreases as S increases. In general, the introduction of swirl reduces shear stress at the wall, while smoothing away the pressure peak at the axis. Both effects are important for surface cleansing or cooling technological applications.

For $S>S^*$, a recirculating VB bubble is observed at the symmetry axis: this reduces drastically the maximum value of the skin-friction and pressure coefficients at the wall. Flows with VB bubbles which are initially steady become unsteady when the swirl intensity or the Reynolds number is increased. The transition from steady to unsteady flow is different depending on the value of δ; if the vortex core radius is large enough the flow becomes purely periodic, while low values of δ are associated with an imperfectly periodic flow.

ACKNOWLEDGMENTS

Comments by Dr. Riesco-Chueca are appreciated. This work is part of the Project "Swirl-Jet Study," supported by the European Commission under Grant No. COOP-CT-2005-017725.

[1]D. J. Phares, G. T. Smedley, and R. C. Flagan, "The wall shear stress produced by the normal impingement of a jet on a flat surface," J. Fluid Mech. **418**, 351 (2000).
[2]M. D. Desphande and R. N. Vaishnav, "Submerged laminar jet impingement on a plane," J. Fluid Mech. **114**, 213 (1982). AQ: #3
[3]N. Didden and C. M. Ho, "Unsteady separation in a boundary-layer produced by an impinging jet," J. Fluid Mech. **160**, 235 (1985).
[4]J. M. Bergthorson, K. Sone, T. W. Mattner, P. E. Dimotakis, D. G. Goodwin, and D. I. Meiron, "Impinging laminar jets at moderate Reynolds numbers and separation distances," Phys. Rev. E **72**, 066307 (2005).
[5]A. Rubel, "Inviscid axisymmetric jet impingement with recirculating stagnation regions," AIAA J. **21**, 351 (1983).
[6]D. J. Phares, G. T. Smedley, and R. C. Flagan, "The inviscid impingement of a jet with arbitrary velocity profile," Phys. Fluids **12**, 2046 (2000).
[7]J. R. Guarino and V. P. Manno, "Characterization of laminar jet impingement cooling in portable computer applications," IEEE Trans. Compon. Packag. Technol. **250**, 337 (2002). AQ: #4
[8]A. Bouafsoun, A. Othmane, A. Kerkeni, N. Jaffrézic, and L. Ponsonnet, "Evaluation of endothelial cell adherence onto collagen and fibronectin: A comparison between jet impingement and flow chamber techniques," Mater. Sci. Eng., C **26**, 260 (2006).
[9]R. N. Vaishnav, H. B. Atabek, and D. J. Patel, "Properties of intimal layer and adjacent flow," J. Engrg. Mech. Div. **104**, 67 (1978).
[10]D. L. Fry, "Responses of the arterial wall to certain physical factors in atherogenesis-initiating factors," *CIBA Foundation Symposium* (Elsevier, Amsterdam, 1973), Vol. 12, pp. 93–125.
[11]J. K. Abrantes and L. F. A. Azevedo, "Fluid flow and heat transfer characteristics of a swirl jet impinging on a flat plate," Begellhouse Proceedings IHTC13, 2006 (■, ■, ■), p. 16.230. AQ: #5
[12]Z. X. Yuan, Y. Y. Chen, J. G. Jiang, and C. F. Ma, "Swirling effect of jet impingement on heat transfer from a flat surface to CO_2 stream," Exp. Therm. Fluid Sci. ■, 55 (2006).
[13]L. Huang and M. S. El-Genk, "Heat transfer and flow visualization experi- AQ: #6

ments of swirling, multi-channel, and conventional impinging jets," Int. J. Heat Mass Transfer **410**, 583 (1998). AQ: #7

[14] R. Gardon and J. C. Akfirat, "The role of turbulence in determining the heat-transfer characteristic of impinging jets," Int. J. Heat Mass Transfer **8**, 1261 (1965).

[15] K. Jambunathan, E. Lai, and M. A. Mossand, "A review of heat transfer data for single circular jet impingement," Int. J. Heat Fluid Flow **130**, 106 (1992). AQ: #8

[16] P. Billant, J. M. Chomaz, and P. Huerre, "Experimental study of vortex breakdown in swirling jets," J. Fluid Mech. **376**, 183 (1998).

[17] T. Loiseleux, J. M. Chomaz, and P. Huerre, "The effect of swirl on jets and wakes: Linear instability of the Rankine vortex with axial flow," Phys. Fluids **10**, 1120 (1998).

[18] M. R. Ruith, P. Chen, E. Meiburg, and T. Maxworthy, "Three-dimensional vortex breakdown in swirling jets and wakes: Direct numerical simulation," J. Fluid Mech. **486**, 331 (2003).

[19] H. Liang and T. Maxworthy, "An experimental investigation of swirling jets," J. Fluid Mech. **525**, 115 (2005).

[20] C. E. Cala, E. C. Fernandes, M. V. Heitor, and S. I. Shtork, "Coherent structures in unsteady swirling jet flow," Exp. Fluids **400**, 267 (2006). AQ: #9

[21] S. V. Alekseenko, A. V. Bilsky, V. M. Dulin, and D. M. Markovich, "Experimental study of an inpinging jet with different swirl rates," Int. J. Heat Fluid Flow **28**, 1340 (2007).

[22] E. Sanmiguel-Rojas, M. A. Burgos, C. del Pino, and R. Fernandez-Feria, "Three-dimensional structure of confined swirling jets at moderately large Reynolds numbers," Phys. Fluids **20**, 044104 (2008).

[23] M. A. Herrada and R. Fernandez-Feria, "On the development of three-dimensional vortex breakdown in cylindrical regions," Phys. Fluids **18**, 084105 (2006). AQ: #10

[24] B. L. Owsenek, T. Cziesla, N. K. Mitra, and G. Biswas, "Numerical investigation of heat transfer in impinging axial and radial jets with superimposed swirl," Int. J. Heat Mass Transfer **490**, 141 (1997).

[25] S. Z. Shuja, B. S. Yilbas, and M. Rashid, "Confined swirling jet impingement onto an adiabatic wall," Int. J. Heat Mass Transfer **46**, 2947 (2003).

[26] J. H. Faler and S. Leibovich, "An experimental map of the internal structure of a vortex breakdown," J. Fluid Mech. **86**, 313 (1978).

[27] J. D. Buntine and P. G. Saffman, "Inviscid swirling flows and vortex breakdown," Proc. R. Soc. London, Ser. A **449**, 139 (1995).

[28] M. A. Herrada, M. Pérez-Saborid, and A. Barrero, "Vortex breakdown in compressible flows in pipes," Phys. Fluids **15**, 2208 (2003).

[29] J. Redding, "Dredging, scouring, excavation and cleaning," U.S. Patent Application No. US 2006/0151631 A1 (■ ■ 2006). AQ: #11

[30] J. M. Lopez and J. Shen, "An efficient spectral-projection method for the Navier-Stokes equations in cylindrical geometries I. Axisymmetric cases," J. Comput. Phys. **1390**, 308 (1998).

[31] R. E. Lynch, J. R. Rice, and D. H. Thomas, "Direct solution of partial differential equations by tensor product methods," Numer. Math. **60**, 185 (1964). AQ: #12 AQ: #13

[32] M. P. Escudier, "Vortex breakdown: observations and explanations," Prog. Aerosp. Sci. **25**, 189 (1988).

[33] J. M. Lopez, "Axisymmetric vortex breakdown Part 1. Confined swirling flow," J. Fluid Mech. **221**, 533 (1990).

AUTHOR QUERIES — 017901PHF

#1 Please check changes in byline
#2 “apart the wall” changed to “the wall apart” — please confirm change is OK
#3 CrossRef reports the author should be ″Deshpande″ not ″Desphande″ in the reference 2 ″Desphande, Vaishnav, 1982″. Please check.
#4 CrossRef reports the volume should be ″25″ not ″250″ in the reference 7 ″Guarino, Manno, 2002″. Please check.
#5 Please supply publisher, city, and year in Ref. 11
#6 Please supply volume number in Ref. 12
#7 CrossRef reports the volume should be ″41″ not ″410″ in the reference 13 ″Huang, El-Genk, 1998″. Please check.
#8 CrossRef reports the volume should be ″13″ not ″130″ in the reference 15 ″Jambunathan, Lai, Mossand, 1992″. Please check.
#9 CrossRef reports the volume should be ″40″ not ″400″ in the reference 20 ″Cala, Fernandes, Heitor, Shtork, 2006″. Please check.
#10 Refs. 23 & 28: Volume number changed. Please check.
#11 Please supply day and month in Ref. 29
#12 CrossRef reports the volume should be ″139″ not ″1390″ in the reference 30 ″Lopez, Shen, 1998″. Please check.
#13 CrossRef reports the volume should be ″6″ not ″60″ in the reference 31 ″Lynch, Rice, Thomas, 1964″. Please check.